AIAA 81-0612R

In-Flight Structural Dynamic Characteristics of the XV-15 Tilt-Rotor Research Aircraft

J. M. Bilger,* R.L. Marr,† and Ahmad Zahedi‡
Bell Helicopter Textron, Fort Worth, Texas

The XV-15 tilt-rotor research aircraft has recently completed the contractor flight test program at the Bell Helicopter Textron Flight Research Center, Arlington, Tex. During these development and envelope expansion flights (60 h of flight, 140 flights), the aircraft has been tested up to a maximum true airspeed of 557 km/h (346 mph, 301 knots). Results of the structural characteristics obtained during this testing are presented. Included is a discussion concerning the rotor and airframe loads, natural frequency placements, airframe control system interaction, and wing/rotor/pylon aeroelastic stability. Measured data are compared with predicted values for many cases.

Nomenclature

B_l = fore and aft flapping angle, deg
BHT = Bell Helicopter Textron
FLT(S) = flight(s)
G.W. = gross weight
HT = horizontal
i_n = nacelle angle (0 deg = airplane, 90-deg = helicopter)
M.L. = monitoring limit
N_R = rotor rpm (100% = 601 rpm)
N/REV = frequency at the Nth harmonic of the rotor (N/Rev, N = 1,2,3, etc.)
OSC = oscillatory
S/N = serial number
V_D = design dive speed
VIAS = indicated airspeed
VT = vertical
YOKE = blade hub at station 9.0 in.
δ_F = flap deflection anglel, deg
ξ = damping coefficient, %
0_L = nacelle at zero angle and in the locked position

Introduction

THE XV-15 tilt-rotor research aircraft was designed, built, and tested by Bell Helicopter Textron (BHT) under a joint NASA/Army/Navy Contract (NAS2-7800). Characteristic of the tilt-rotor aircraft is a 25 ft diam, three-bladed rotor mounted on each wing tip (Figs. 1 and 2). The nacelles, which contain the rotor/pylon, engine, and transmission are attached to the wing by the conversion spindle and can be tilted from 95 to 0 deg. The 90 deg position is the helicopter mode. The 0 deg position is the airplane mode. Positions in between are referred to as tilt-rotor mode. The rpm of the rotor can be varied between 438-601 rpm or 7.3-10 Hz at 1/rev frequency. Currently, normal operation is 517 rpm in the airplane mode and 589 rpm in the helicopter and tilt-rotor modes. These settings are currently being set by structural load criteria, not by performance and/or crew comfort criteria. The effort to place the various structural modes away from resonances to allow usage of the rpm range, along with flight test results, will be discussed.

Presented as Paper 81-0612 at the AIAA Dynamics Specialists Conference, Atlanta, Ga., April 9-10, 1981; submitted April 24, 1981; revision received Dec. 21, 1981.

*Principle Structural Dynamic Engineer, Tilt Rotor Program.
†XV-15 Senior Test Project Engineer.
‡Experimental Stress Engineer, Tilt Rotor Program. Member AIAA.

Also of importance in the tilt-rotor evaluation is the wing/rotor/pylon aeroelastic stability in airplane mode. The procedures used to obtain this information and the methods used to analyze these data are discussed. The flight results compared with calculated data will be presented for six stability modes during level flight and for windmilling rotors. Also discussed is the effect of the control system interaction on the aeroelastic stability, primarily for the antisymmetric wing beam mode.

The other significant structural characteristic to be discussed is the effect of the rotor/nacelle wake on the empennage.[2]

Dynamic Components and Airframe Natural Frequencies

Rotor

The coupled natural frequencies of the rotor were predicted using a Myklestad analysis that includes the elastic and inertial coupling between bending (beam, chord, and torsion) and the flexibility of the control system. The resulting rotor natural frequencies are shown in Figs. 3 and 4 in terms of collective and cyclic modes, respectively. Collective modes have polar symmetry about the mast and cyclic modes are antisymmetric with respect to the mast. As shown, only two significant modes were predicted to be in or near resonance. These were the third collective mode and the second cyclic mode.

The third collective mode (near 6/rev) is excited at high rotor rpm and at high blade collective pitch in the helicopter mode. The second cyclic mode (near 4/rev) approaches resonance in the airplane mode with the nacelles locked and as the blade collective pitch increases at low rotor rpm. During the test program (both wind tunnel and flight), these conditions were monitored but did not present any rotor loading problem. The second cyclic mode is shown in Fig. 5 as the 4/rev loading to the yoke chord bending. The rotor natural frequencies measured during flight agree with predictions.

Airframe

The airframe structure natural frequencies were predicted using the NASA structural analysis program (NASTRAN). A detailed model of the wing/pylon interface, including details of the pylon assembly, was developed to analyze the effects of pylon component stiffnesses on the coupled frequencies and responses. Computer models of the complete airframe, similar to that shown in Fig. 6, were used to calculate the fuselage and empennage natural frequencies and to investigate the influence of the wing-to-fuselage stiffness on the

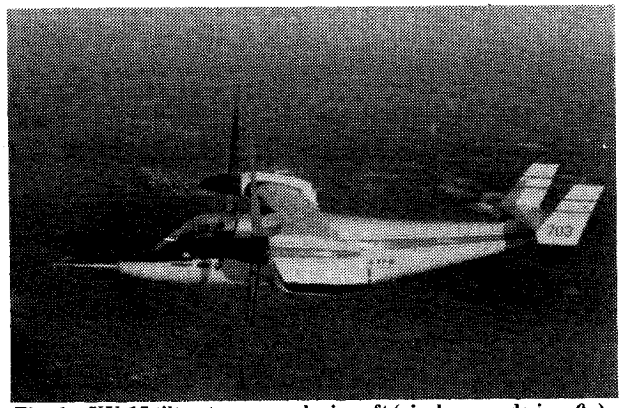

Fig. 1 XV-15 tilt-rotor research aircraft (airplane mode $i_n = \theta_L$).

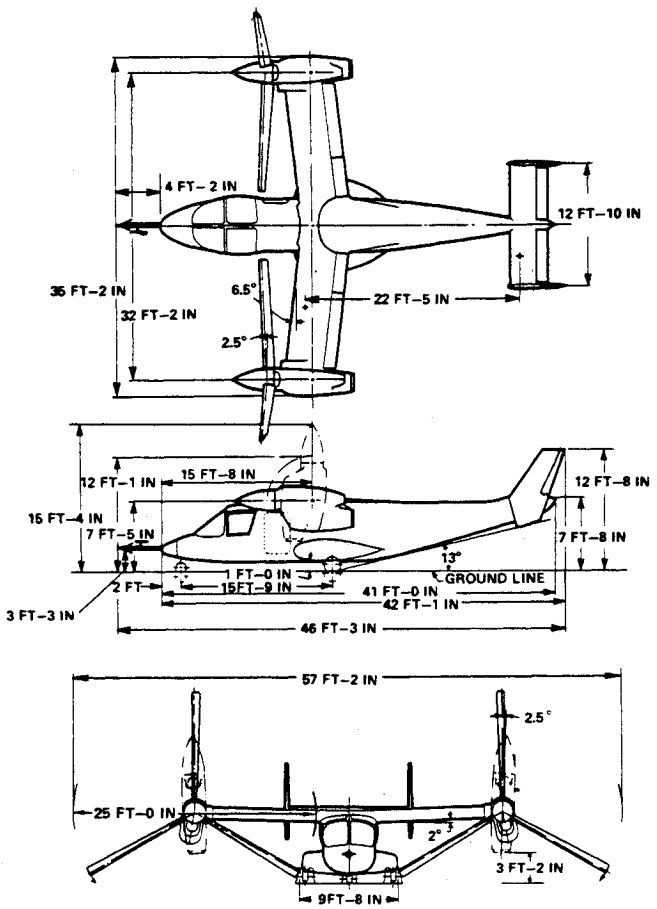

Fig. 2 XV-15 tilt-rotor research aircraft: three-view drawing.

wing/pylon natural frequencies. The calculated natural frequencies of the airframe as a function of nacelle angle are presented in Fig. 7 for symmetric and antisymmetric modes.

The gradual natural frequency variation with the nacelle angle is due to the shift in the location of the pylon mass as the nacelles are converted. Since the nacelles comprise approximately 40% of the empty weight, this effect is significant. The sudden change in natural frequencies at nacelle angles of 0 deg is due to the engagement of the pylon downstop. The downstop provides an additional load path between the transmission and the wing. Therefore, the frequencies of the modes that involve pylon pitching or yawing with respect to the wing are significantly influenced by whether the pylon is on or off the downstop. One of the structural modes that was predicted to be near resonance with the rotor excitation is the pylon lateral mode at high rotor rpm, on the downstop, and near rotor 2/rev.

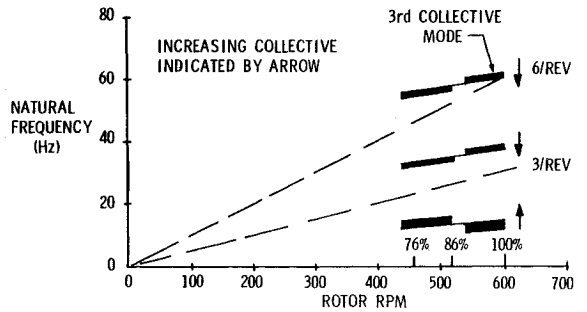

Fig. 3 Rotor natural frequencies collective mode.

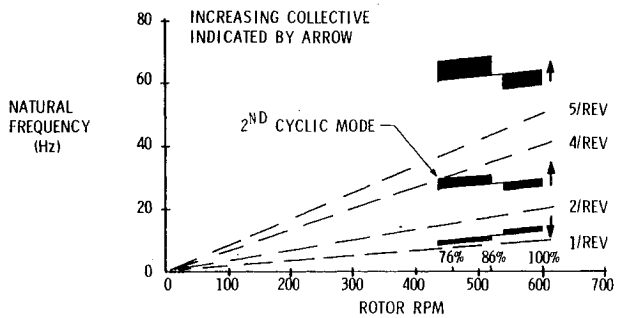

Fig. 4 Rotor natural frequencies cyclic mode.

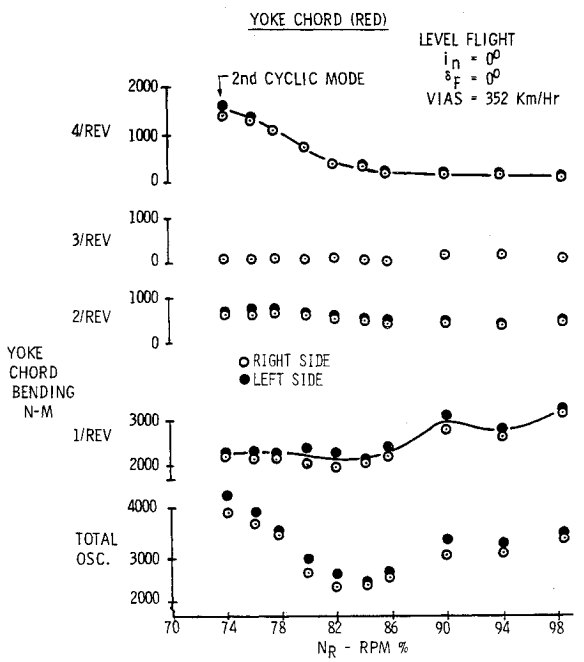

Fig. 5 XV-15 rotor loads (*ST* 9.0).

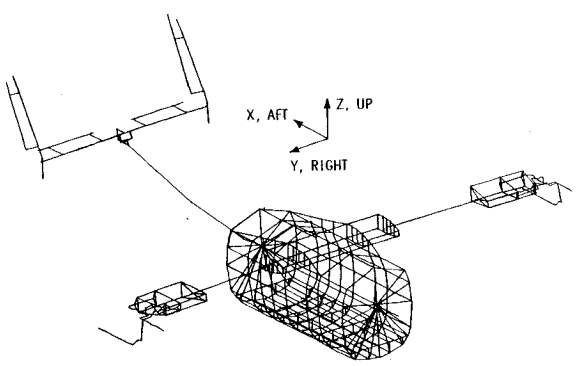

Fig. 6 Finite-element model used to calculate airframe natural frequencies.

Pylon

The pylon lateral mode natural frequencies were predicted to be 19.5 and 19.0 Hz for symmetric and antisymmetric modes, respectively. The symmetric mode was measured to be slightly lower during flight at 18.0 Hz, as shown in Fig. 8; however, the antisymmetric mode was never located. The pylon lateral mode shape and natural frequency change depending upon whether the pylon is locked (airplane mode) or unlocked. When the pylon is unlocked (off the downstop), the mode shape is primarily a rigid body pylon yawing about the conversion spindle. The source of excitation is from the same conditions affecting rotor track and balance that produce a 1/rev loading in the fixed system. This loading primarily affects the conversion spindle and requires good rotor track and balance.

The pylon lateral mode, on the downstop, is predominantly pylon lateral bending and roll motion with very small engine c.g. motion. For this mode, the sources of excitation from the rotor are the Hook's joint effect and the rotor second cyclic mode producing a fixed system response at 2/rev (18 Hz) and 3/rev (23.5 Hz), respectively. This results in the increased loading to the conversion spindle and downstop as shown in Figs. 9 and 10. NASTRAN analysis has shown that by reducing the lateral stiffness of the downstop the pylon lateral mode can be lowered significantly. This would then eliminate, within the operational rpm range, the 2/rev loading on the conversion spindle and both the 2/rev and 3/rev loadings on the downstop. Currently, flight tests are planned to investigate the effects of reduced downstop lateral stiffness on this mode.

Engine

The engine yaw and pitch modes were predicted to be nominally free from resonance within the operational rpm ranges, but measurements taken during flight showed the natural frequencies to be 4-5 Hz higher, locating this mode within the operational rpm range. Harmonics for the engine coupling gearbox yawing moment and pitch strut load are shown in Figs. 11 and 12. The 2/rev (15.2 Hz) loading is from the engine yaw mode and its source of excitation is also from Hook's joint effect. The engine yaw mode is predominantly engine c.g. lateral motion with some pylon lateral and roll motion. This loading affects both the pitch strut and engine coupling gearbox. The 3/rev loading is from the engine pitch mode, which receives its source of excitation from the rotor 3/rev, causing loading only on the engine pitch strut.

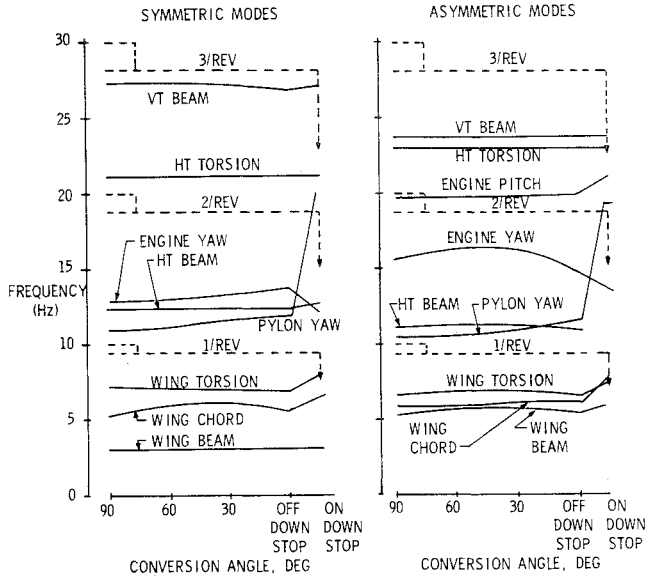

Fig. 7 Calculated structural natural frequencies.

The engine yaw mode is sensitive to flapping angle and can be controlled by reducing the amount of flapping for any given configuration. This was accomplished by rigging the fore/aft swashplate down 1.5 deg and optimizing the lateral swashplate to 0.5 deg inboard. Both changes result in a near-zero flapping condition during high-speed forward flight. The resulting reduction in 2/rev loading is illustrated in Figs. 11 and 12.

Aeroelastic Stability

General

Aeroelastic stability data for the wing/pylon/rotor system were obtained using three excitation techniques: exciter frequency sweeps (automatic), atmospheric turbulence (RANDOMDEC), and exciter frequency dwells (decay method).

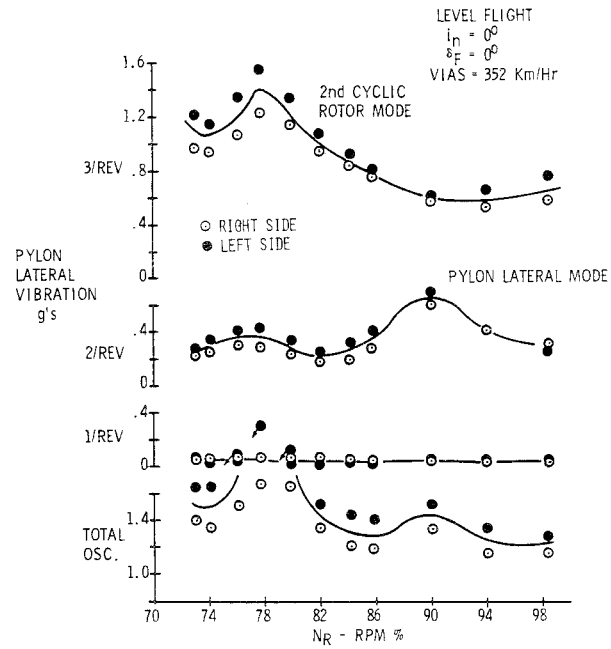

Fig. 8 XV-15 pylon vibrations.

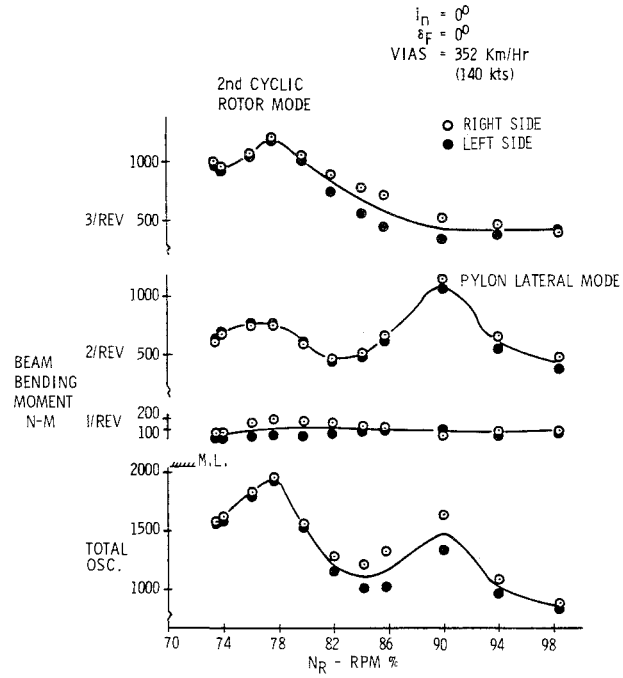

Fig. 9 XV-15 conversion spindle loads.

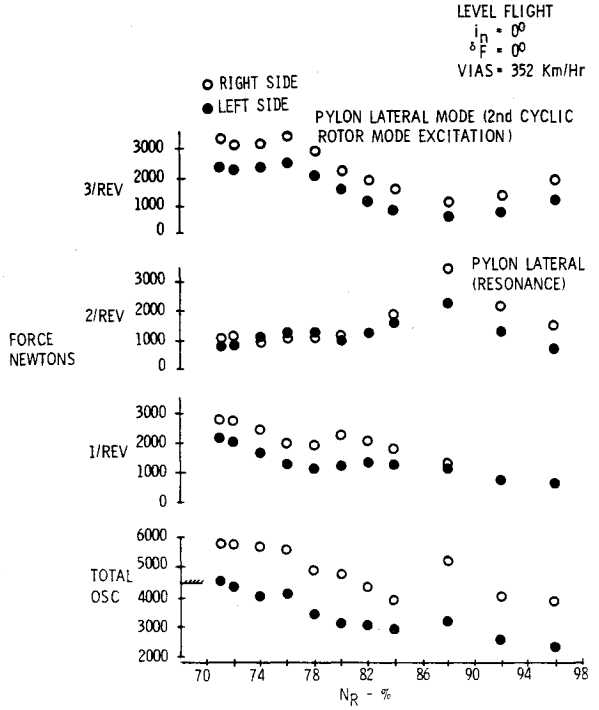

Fig. 10 Pylon downstop vertical force vs M/R rpm.

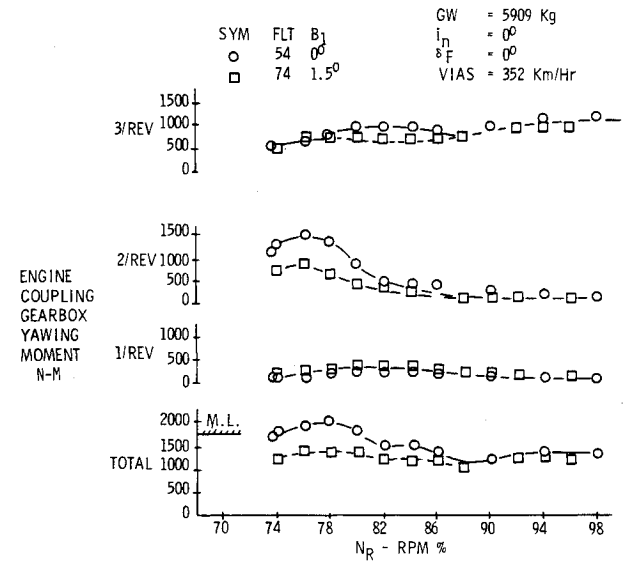

Fig. 11 XV-15 engine coupling gearbox loads.

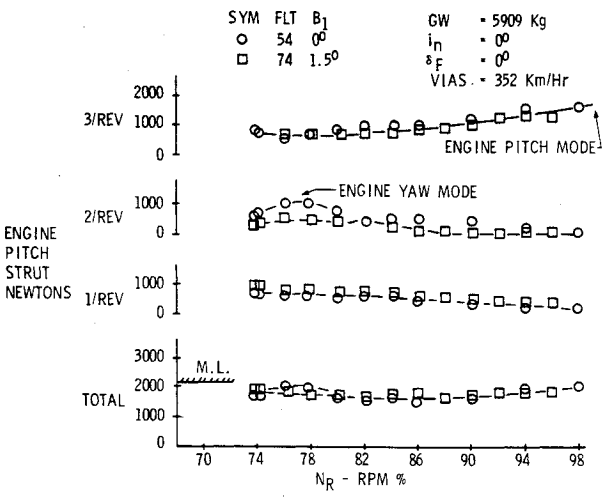

Fig. 12 XV-15 engine pitch strut axial load.

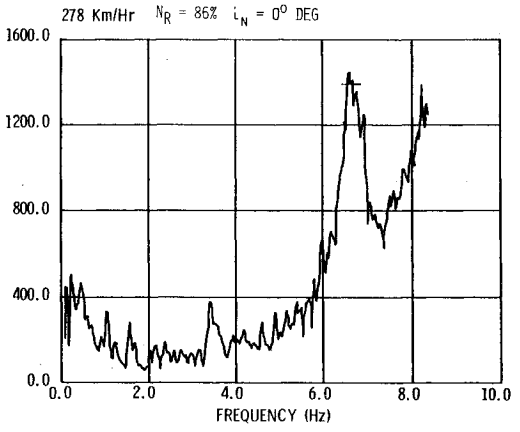

Fig. 13 Symmetric wing chord bending, in.-lb (sweep).

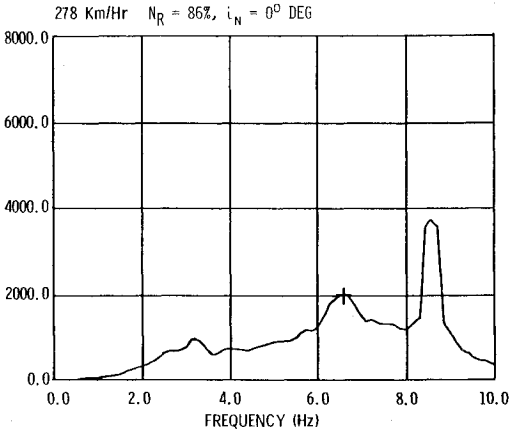

Fig. 14 Symmetric wing chord bending, in.-lb (turbulence).

The inflight excitation consists of rotor collective and flaperon control inputs. Strain gages are mounted at the wing elastic axis to measure the beam bending, chord bending, and torsion response. The left and right gages were combined in a sum/difference network to separate the symmetric and antisymmetric modes.

Frequency response functions using the standard fast Fourier transform (FFT) technique were determined from the airframe response to the frequency sweeps and turbulence. Examples are shown in Figs. 13 and 14. Constant frequency dwells and decays were then performed at the noted airframe natural frequencies to obtain the free decay of the modal response as shown in Fig. 15a. During the flight, these decays were monitored and quick-look damping data were estimated, as required, using the logarithmic decrement of the hand-drawn decay envelope. In addition, the free decay response was also determined using the RANDOMDEC technique[3] on the airframe response to turbulence as shown in Fig. 15b. In both cases, the free decay sometimes included airframe response to rotor 1/rev that shows up as a constant amplitude oscillation.

These decays were analyzed using an interactive computer program to obtain the modal damping. The program was sometimes used in real time during the flight to obtain damping data for a preselected mode. Due to the amount of data taken on any given flight, it was necessary to perform most of the damping analysis after the flight. Damping and

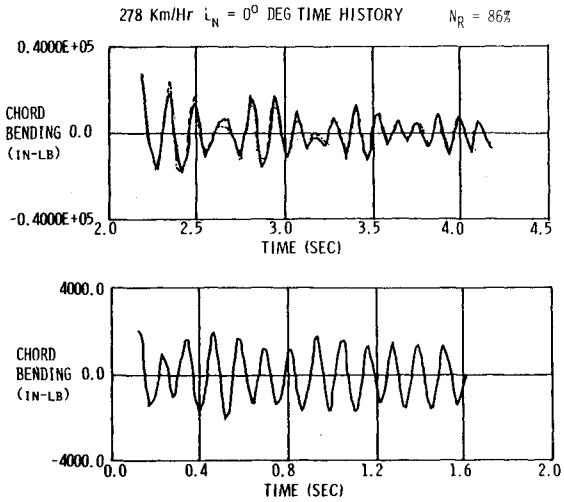

Fig. 15 Frequency decay plots: a) symmetric wing chord constant frequency dwells, in.-lb; b) symmetric wing chord decay from turbulence, in.-lb.

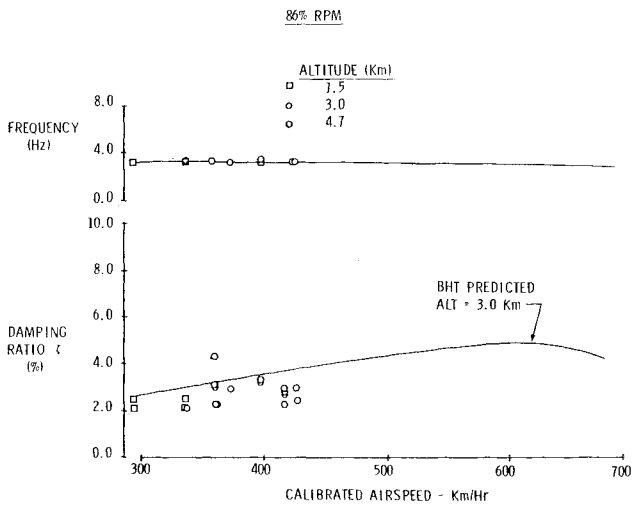

Fig. 16 Symmetric wing beam bending.

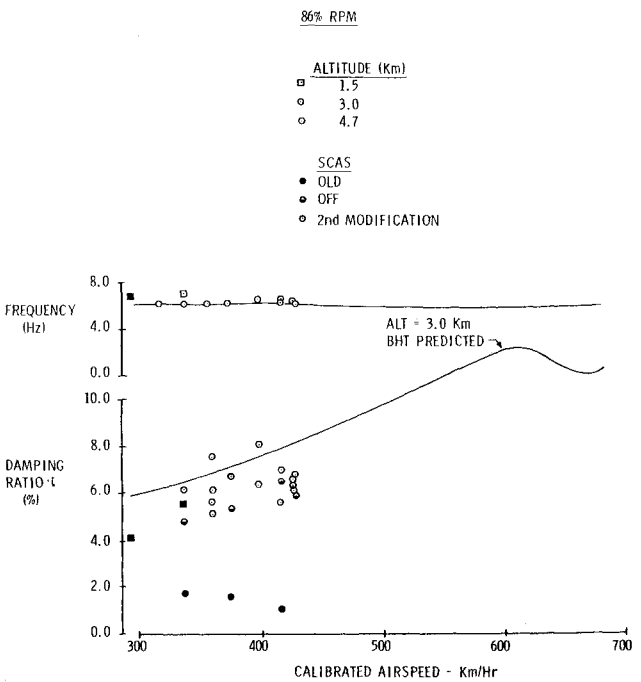

Fig. 17 Antisymmetric wing beam bending frequency.

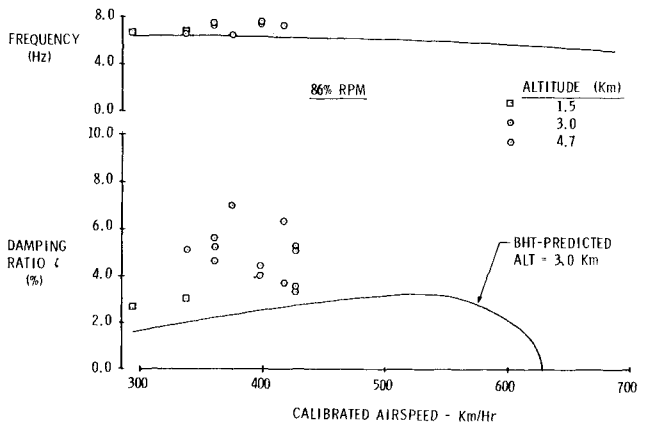

Fig. 18 Symmetric wing chord bending.

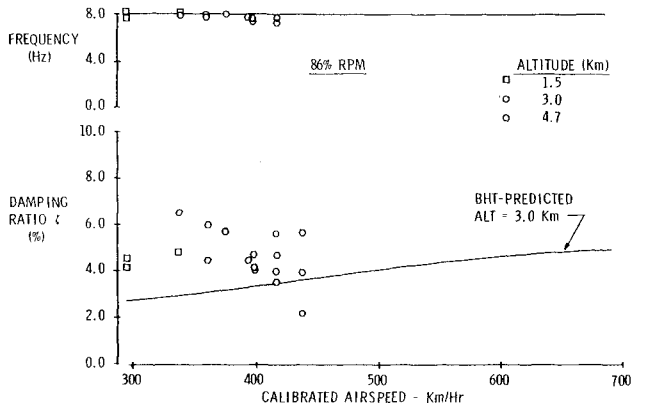

Fig. 19 Antisymmetric wing chord bending.

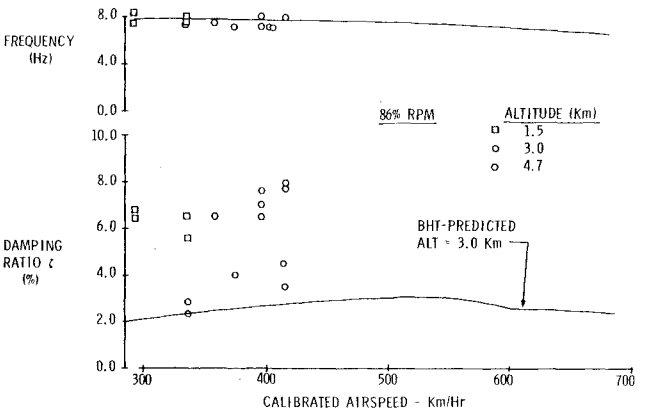

Fig. 20 Symmetric wing torsion.

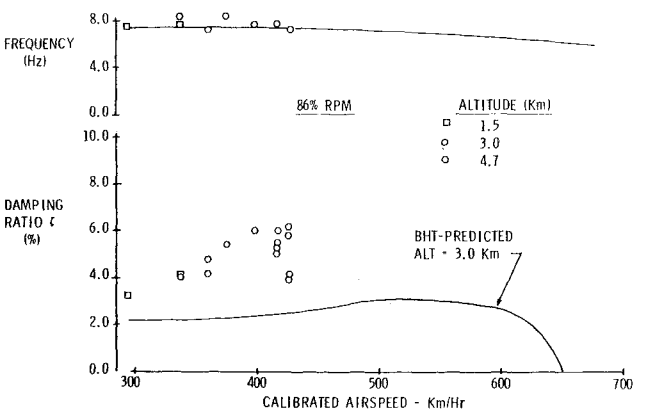

Fig. 21 Antisymmetric torsion.

frequency vs airspeed plots were continually updated as the airspeed and altitude envelope was expanded.

Analysis

The model for the damping analysis uses a series of exponential functions with constant complex coefficients to represent the decay response

$$X(t) = \sum_{i=1}^{m} A_i e^{a_i t} \quad (1)$$

This expression can be used to approximate or curve fit time-history responses that are composed of terms such as $Be^{\xi t}$ (critically damped), $Be^{\xi t}\cos\omega t$ (damped sinusoid), and $B\cos\omega t$ (constant amplitude sinusoid) which commonly appear in flight flutter testing.

The wing response data were conditioned through a bandpass filter prior to being digitized for analysis. Using finite-difference equation techniques, the time series of data samples taken for the decay were used to compute the unknowns A_i and a_i of Eq. (1) by least squares curve fitting of the analytical model. The number of terms used in the approximation will vary depending on the number of significant modal decays or rotor harmonics present in the data. Also inherently assumed is that there are no other significant transient forcing functions present once the constant frequency excitation is removed.

Results

Data were taken for 2 rpm, 98 and 86%, and three altitudes (1.5, 3.0, and 4.7 km). Plots of natural frequency and damping vs airspeed were made for the first six wing/pylon modes, comparing calculated and measured values. Examples are presented in Figs. 16-21 for 86% rpm. Due to rotor limits, a maximum speed of 374 km/h (202 KCAS) was obtained at 98% N_R. At 86% N_R, data have been taken at a maximum speed of 424 km/h (229 KCAS), which is 558 km/h (301 KTAS) true airspeed.

The measured natural frequencies agreed very well with predictions. The measured damping was higher than predicted except for the wing beam modes. The measured damping of the symmetric beam mode is only slightly lower than predicted and it shows an increasing trend with airspeed. The antisymmetric beam mode damping at 3.0 km altitude was considerably lower than predicted as shown in Fig. 17. An investigation showed that the roll stability and control augmentation system (SCAS) was coupling with the structural mode to continue driving the oscillations after the original excitation was removed. Turning the SCAS off eliminated the problem, thus verifying the adverse coupling effect. The open-loop aircraft roll response to flaperon input was measured to determine the system gain and what changes would be necessary. The SCAS system was then modified by adding a notch filter circuit to attenuate the SCAS response to the structural mode at 6 Hz. The actuator break frequency was also lowered electronically to offset the phase changes due to the notch filter. Subsequent testing with this modification showed that the new damping data are close to prediction.

Comparisons were made between the damping results obtained from the decays generated by RANDOMDEC and the frequency dwells at 98% N_R. These results agreed quite well, as shown in Fig. 22. Either of the two techniques could be used depending on the level of turbulence during the test. The dwell method requires very smooth air to obtain the best results, whereas RANDOMDEC works better with high levels of turbulence, especially in the presence of rotor harmonic excitation. Due to the proximity of rotor 1/rev at 86% N_R to the higher frequency wing modes and the low level of turbulence encountered at the time of testing, the RANDOMDEC method was not used when expanding the airspeed altitude envelope at 86% N_R. The initial use of this method and its agreement with the dwell method did give confidence to the continued use of the dwell method.

Damping analysis using swept sine techniques was attempted but was not successful, since not enough energy could be introduced into the modes to produce good results.

Empennage

Empennage structure oscillatory loadings, which required modification of the structure, were encountered during full-scale wind-tunnel testing.[2] The loading was identified as being induced by wing/pylon/rotor vortices with the potentially damaging loads being impulsive in nature and resulting in symmetric and antisymmetric modal response at the empennage.

An analysis was performed to determine the loads in the empennage structure during the modal response. Inertial loading was determined for the various modes using the simple dynamic model. The predicted modes of the empennage using this model agree very well with the measured modes. The resulting shears, moments, and torques were collocated to selected points on a detailed static model and the resulting stresses throughout the structure were calculated. The allowable bending moment at a selected station for the symmetric or antisymmetric response was determined and structural modifications made so that the endurance limit would not be exceeded at any point in the structure. This allowable bending moment was selected based on results of the full-scale wind-tunnel test.

The first 15 flights were devoted primarily to the evaluation of the empennage loads. The flight envelope was expanded in nacelle angle increments of 5 deg from 90 to 60 deg (the range in which the highest loads were encountered in the wind tunnel). At each conversion angle, sideslips, turns, climbs, and descents were made at each nacelle angle and airspeed. The empennage loads recorded during level flight are

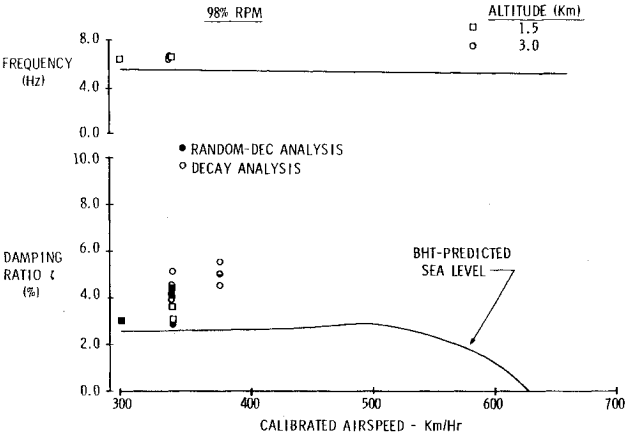

Fig. 22 Symmetric wing chord bending.

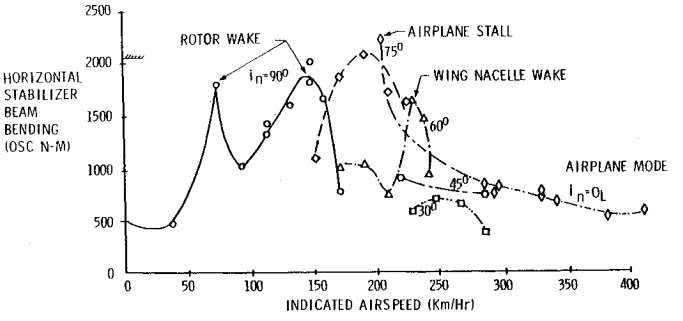

Fig. 23 XV-15 empennage loads due to rotor wing/nacelle wake and tail buffet.

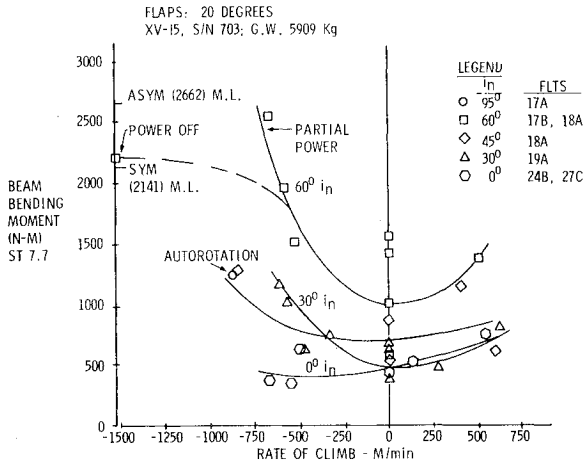

Fig. 24 Horizontal stabilizer bending moment.

presented in Fig. 23. The turn and sideslip conditions had little effect on empennage loads.

The level flight load peaks at different airspeeds depending on conversion angle. The empennage loading during low speed in the helicopter mode is due to the rotor tip vortex hitting the empennage. The characteristics of the rotor vortex that impinges on the empennage in the speed range of 37-93 km/h (20-50 knots) are quite different from those at other flight regimes. Below 37 km/h, the rotor wake has little effect on the empennage. Between 37 and 93 km/h, the rotor wake reacts more like the wake of a highly loaded low-aspect-ratio wing exciting the empennage antisymmetric mode natural frequency. The rotor wake produces a random "whipping" impulsive loading on the empennage and is dependent upon power, aircraft attitude, and wind conditions.

Above 93 km/h and conversion angles to 70 deg the rotor wake frequency on the empennage becomes predominantly 3/rev (blade passage). The loading due to this condition increases or decreases depending on the combination of airspeed, nacelle angle, and aircraft attitude to position the rotor wake on the empennage. At 60 deg nacelle angle, the higher loads are more random at the empennage symmetric mode natural frequency. This loading is induced by the wing/nacelle vortex and appears in level flight to be isolated between 204 and 241 km/h.

For nacelle angles less than 60 deg, the loads are reduced. The 3/rev and wing/nacelle vortex become insignificant at the lower nacelle angles, and the oscillatory loading is from normal wing/nacelle wake and turbulence. However, when approaching wing stall, the turbulence due to flow separation causes impulsive loading on the empennage, resulting in symmetric beam modal response.

The empennage loads measured during climb and descents are presented in Fig. 24. Empennage loads increase significantly with rate of descent (as angle of attack is increased). This type of empennage loading, which produces the highest loads, is from a vortex that originates from the gap between the wing tip and nacelle. The strength of the vortex increases with nacelle angle as the nacelles are converted from the airplane mode and also as angle of attack is increased. This vortex combines with the wing tip vortex and is pulled inboard due to the nacelle cross-sectional camber. This vortex produces a random oscillatory/impulsive loading on the upper portion of the vertical stabilizer exciting the symmetric beam mode of the empennage. As the angle of attack is increased, the loading on the empennage increases. This loading was the highest for nacelle angles between 75 and 60 deg where the combination of wing/nacelle gap, airspeed, and rotor wake were the most significant. Loads were measured up to the monitoring limit during a simulated power-off descent 1524 m/min (5000 ft/min) at 60 deg nacelle angle. For rates of descent less than 610 m/min (2000 ft/min), the empennage loads were below the monitoring limit for all nacelle angles. In approaching rates of descent between 549 and 610 m/min (1800 and 2000 ft/min) or wing stall, the loading can be felt by the pilot through increased aircraft vibration and sound level which permits him to avoid the higher load conditions.

Conclusions

Structural characteristics have not limited the development of a usable flight envelope to demonstrate the proof of concept of the tilt-rotor aircraft.

Significant structural modes have been identified and several possible solutions to relocate frequencies and reduce loading have been analytically evaluated. Some of these modifications have been flight tested and appear promising. Evaluation of the remaining modifications is planned to continue through flight testing at Dryden Flight Research Center and NASA Ames Research Center during the latter part of 1980.

Aeroelastic stability data taken during level and windmilling flight to date agree well with prediction. Additional testing up to design dive speed V_D is planned to determine if any trend toward an instability exists within the flight envelope and for correlations with the flutter predictions.

References

[1] Wernicke, K. and Magee, J., "XV-15 Flight Test Results Compared with Design Goals," AIAA Paper 79-1839, 1979.

[2] Marr, R.L., Blackman, S., Weiberg, J.A., and Shroers, L.G., "Wind Tunnel and Flight Test of the XV-15 Tilt Rotor Research Aircraft," AHS 79-54, May 1979.

[3] Cole, H.A. Jr., "On-Line Failure Detection and Damping Measurement of Aerospace Structures by Random Decrement Signatures," NASA CR-2205, March 1973.